
# Contact area measurement of micron-sized metal-coated polymer particles under compression

Molly Bazilchuk , Takashi Sumigawa , Takayuki Kitamura , Zhiliang Zhang , Helge Kristiansen , Jianying He

PII: S0020-7403(18)32842-X
DOI: https://doi.org/10.1016/j.ijmecsci.2019.105214
Reference: MS 105214

To appear in: *International Journal of Mechanical Sciences*

Received date: 29 August 2018
Revised date: 30 September 2019
Accepted date: 4 October 2019

Please cite this article as: Molly Bazilchuk , Takashi Sumigawa , Takayuki Kitamura , Zhiliang Zhang , Helge Kristiansen , Jianying He , Contact area measurement of micron-sized metal-coated polymer particles under compression, *International Journal of Mechanical Sciences* (2019), doi: https://doi.org/10.1016/j.ijmecsci.2019.105214

**Highlights**

- In conductive adhesives, compressed metal-coated polymer spheres form electrical contact.
- The contact area in the sphere-plate problem is not well studied experimentally.
- Using nanoindentation in scanning electron microscope the contact area was measured.
- The measured contact area was used to validate several analytical models.

# Contact area measurement of micron-sized metal-coated polymer particles under compression

Molly Bazilchuk[1,2], Takashi Sumigawa[3], Takayuki Kitamura[3], Zhiliang Zhang[1], Helge Kristiansen[1,2] and Jianying He[1*]

[1] *Department of Structural Engineering, Norwegian University of Science and Technology (NTNU), Trondheim, 7491, Norway*

[2] *Conpart AS, Skjetten, 2013, Norway*

[3] *Department of Materials Science and Engineering, Kyoto University, Kyoto, Japan*

**Corresponding author: jianying.he@ntnu.no*

Keywords: Nanoindentation, conductive adhesives, contact area

## Abstract

The contact problem of a sphere under compression by a rigid plate is pertinent to understanding electrical contact formation in anisotropic conductive adhesive (ACA) applications. However, no work has experimentally verified existing contact models for the metal-coated sphere-plate contact problem. Herein, compression tests on metal-coated polymer spheres were performed by flat punch nanoindentation with in-situ scanning electron microscopy (SEM) monitoring, and the resultant contact area was measured using SEM images. The obtained results were compared to Tatara and Abbott-Firestone models, along with finite element analysis (FEA). The measured contact area falls between Tatara and Abbott-Firestone models, indicating a mixture of elastic and plastic deformation. The contact area as a function of force is dominated by the polymer core and independent of the metal coating for the thin metal coatings tested. The work provides guidelines for bonding parameters for ACA assembly.

## 1. Introduction

The classic mechanics problem of a sphere compressed between two plates has been studied for over a century, and is still considered one of the grand challenges of particle technology [1,2]. Hard coatings are used in a variety of applications to protect softer substrates, and local asperities can be modelled as spheres in order to understand deformation of microscopically rough surfaces under pressure [3,4]. The sphere-plate contact problem is particularly relevant in analyzing anisotropic conductive adhesives (ACA), which are applied in electronics packaging. In ACA, unidirectional electrical contact is formed through conductive particles dispersed in adhesive [5]. The particles conduct only when compressed between corresponding bumps. Understanding and thereby optimizing the contact resistance through individual conductive particles will allow for joint resistance to be minimized, enabling finer pitches and more reliable interconnect.

Metal-coated polymer particles (MPS) in the size range 3-10 μm are often used as the conductive component in ACA. MPS are microcomposites, combining the mechanical compliance of

a polymer core with electrical conductance of a thin metal coating. Due to the small size of the particles relative to the surfaces they connect, the electrical resistance through the contact area between the particles and the bumps is significant in the overall joint resistance. To minimize the joint resistance, the contact surface should be as large as possible at a given pressure. However, overcompression will compromise the mechanical integrity and thus the reliability of the interconnect [6–8]. MPS are subject to large deformations in excess 20% nominal strain in ACA applications, whereas small strains are commonly considered in contact analysis literature [9].

The large deformation behavior of different types of polymer and MPS has been studied extensively by He et al. [10–12]. Recently, a flat punch nanoindentation technique for simultaneously measuring the electrical resistance and mechanical properties of MPS under compression has been developed [13]. The electrical resistance measured using electromechanical nanoindentation can be considered as the sum of contact resistance through the MPS interfaces, a shell resistance through the metal coating, and resistance through the flat punch and nanoindentation substrate. In this work, we consider the contact resistance, in particular the size of the contact area.

The contact area between bodies can be measured in several ways. Techniques are typically divided into in-situ and ex-situ [14]. In-situ methods include optical, thermal, electrical and acoustic methods. Optical, thermal and acoustic techniques may provide accurate results but are limited in resolution by the wavelengths used to probe the samples [15]. The measurement of electrical contact resistance is a non-destructive and potentially accurate method but requires detailed knowledge about the electrical resistivity of the contacting bodies. As demonstrated in [16], the resistivity of the metal coatings may deviate greatly from bulk properties, so contact resistance is not a valid method to determine the contact area of the MPS.

Ex-situ methods consist of relocating the contact area and measuring with a microscope or profilometer, sometimes employing a third body between the contacting bodies [17]. Due to the small size and softness of the MPS, even a very thin third body would be expected to influence the contact mechanics. In this work, an ex-situ method employing scanning electron microscope is introduced to estimate the contact area between an MPS and a hard indenter tip.

FE modelling allows the implementation of elastic-plastic sphere-plate contact models [9]. Chang et al [18] and Kogut et al. [4] fit FE models to empirical equations which only require the elastic constants and material yield strength. However, these models are discontinuous at the transition between elastic and plastic deformation. Furthermore, in the case of an MPS it is not clear whether the yielding of the polymer core or the metal coating will dominant the size of the contact area. The Etsion group has analyzed coated sphere-plate contacts, which are more relevant for the MPS case since they consist of spherical materials with two layers of different hardness [3,19,20]. Their results only apply to small strains, and validity at higher strains is not considered. To understand the deformation of MPS in ACA applications, understanding large strain characteristics is necessary. We therefore present a complementary FEM analysis to interpret the experimentally determined contact area.

## 2. Theory

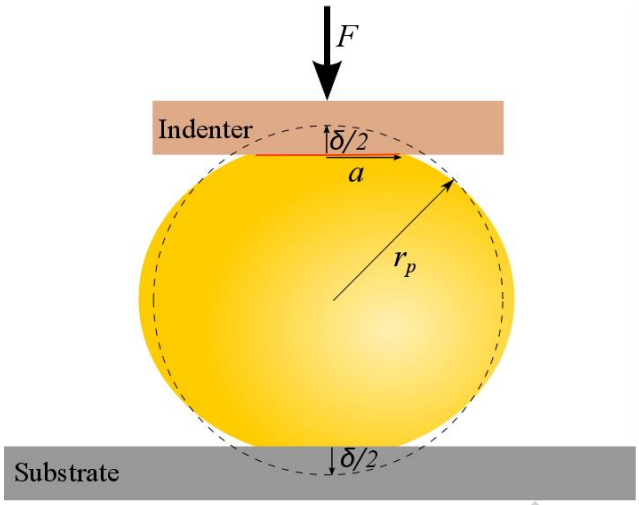


*Figure 1: An illustration of the sphere-plate contact problem for the current system and the variables involved. A compressive force F is applied (e.g. with an indenter) to a sphere of undeformed radius $r_p$ and results in a deformation $\delta$. The contact area between the sphere and the plate can be expressed in terms of a contact radius a.*

The quasi-static sphere-plate contact problem is illustrated in Figure 1. The resultant stress distribution is non-uniform, and as such analysis is not straightforward. For a polymer sphere, the degree of plastic relative to elastic deformation will depend on material factors such as the cross-linking density of the polymer [21]. We therefore consider the two extremes: pure plastic and pure elastic deformation.

The first solution to the sphere-plate contact problem is the Hertz model, which applies in the case of small elastic deformations up to approximately 1% strain [1]. The Tatara model, which expands on the Hertz model by using different boundary conditions, extends validity up to 20% strain [22,23]. In our treatment, we assume that the contacts deform symmetrically, so that the deformation is shared equally on either side of the sphere. The radius of the contact area between the sphere and plate according to both the Hertz and Tatara model may be expressed as:

$$a = \sqrt{r_p \frac{\delta}{2}} \tag{1}$$

where $r_p$ is the undeformed particle radius and $\delta$ the absolute deformation of the sphere as illustrated in Figure 1. Note that the calculation of the contact radius does not require the input of material parameters for this model. This elastic model applies to a homogenous sphere rather than sphere with a stiffer shell and a softer core as we examine in this work. The Johnson elastic model considers friction in the contact region, which adds shear stress and may reduce the contact area [24]. However, this model requires more input parameters and is also only valid for small strains.

The simplest model of a plastic plate-sphere contact is the Abbott-Firestone model, which expresses the radius of the contact area between the sphere and the plate as the geometric overlap of the two, given by [25]:

$$a = \sqrt{r_p \delta} \tag{2}$$

Once again, the contact model does not require the input of any material parameters. It should be noted that this model assumes that the material volume is not conserved under compression. Essentially, the top of the sphere is cut off to the appropriate deformation.

The polymer cores of the MPS in question are known to be viscoelastic [11, 21], although the viscoelastic constants have not been determined. The Poisson's ratio of viscoelastic 260 µm uncoated resorcionol-formaldehyde polymer particles has been studied, and the Tatara model has been found to give the most reasonable prediction [26]. The plate-sphere problem for viscoelastic materials has been studied analytically, however the classic works consider a rigid sphere against a viscoelastic half-space [27–29], while our case is the inverse. Additionally, the analytical models consider small deformations while large deformation analysis is required to interpret the current data. In this work, MPS are evaluated at a constant displacement rate of 100 nm/s, so other viscoelastic effects may be present, they are at least equivalent for all particles studied.

All real contact areas are rough, and contacts are often described in terms of a-spots, or regions were asperities touch to form the current-carrying path in the contact surface [30]. We distinguish between the real (current-carrying) contact area, and apparent contact area, which is the entire region where two bodies ostensibly are in contact. Previous estimate puts the real contact area as a small fraction of the apparent contact area [31]. In his seminal work on electrical contacts, Holm found that the real contact area $A_b$ can be expressed as [32]:

$$\frac{P}{A_b} = \xi H \tag{3}$$

where $P$ is the load (force) on the contact, $H$ the material contact hardness and $\xi$ a value between 0 and 1, where values of 0.1 - 0.3 are common. This applies generally to two contacting bodies of arbitrary shape.

## 3. Materials and Methods

### 3.1. Particles

Conpart AS (Skjetten, Norway) provided MPS for testing in this study. All the MPS consisted of a 9.7 µm [1] core made of styrene cross-linked with 20% DVB. The metal coatings were manufactured using electroless plating. Since the cores were all from the same batch of polymer, the MPS are referred to by their metallization and nominal coating thickness in nanometers, e.g. Au40 means an MPS with a 40nm gold coating. Contact area measurements were performed on the

[1] Coefficient of variance < 2%, as measured by Coulter counter

following types of MPS: Au40, Ag60, Ni90 and Ni120. The metal coating thicknesses are typical values manufactured by Conpart AS. The MPS were dispersed in ethanol and then dried onto a silicon wafer substrate.

### 3.2. Compression testing

Compression tests were performed using a PicoIndenter 85L (Hysitron, Minneapolis, USA) mounted in a Hitachi SU8230 (Tokyo, Japan) SEM. A custom diamond flat punch, 20 µm in diameter, was fabricated from a conical indenter using a focused ion beam. Each compressed MPS was identified on a coordinate system that was used to relocate the same particles in a Hitachi S 5500 SEM for imaging of the contact area from above. SEM imaging was performed in secondary electron (SE) mode to maximize topographic contrast.

The flat punch was manually stepped towards the surface of the MPS until the force gauge on the PicoIndenter unit indicated that the tip had touched the MPS. The punch was then retracted, and the compression test was started 100-500 nm above the point of first contact. The measurements were performed in displacement control, so each particle was deformed at 100 nm/s constant rate up to a set maximum displacement. Loading rates from 10 to 1000 nm/s were tested but statistically significant variations in the measured contact area were not identified. The maximum displacement of the punch was varied systematically from 1000 to 5000 nm for different particles to obtain force/deformation-contact area characteristics. Since the measurement started slightly above the surface of the particle, the maximum recorded deformation of the particles was always slightly less than the specified absolute displacement (e.g. a maximum absolute punch displacement of 5000 nm might give a maximum particle deformation of 4500 - 4900 nm). The force was measured continuously during compression.

### 3.3. Contact area measurement

A shaded area was visible in the micrographs of the MPS that had been compressed. Since there was no such region on untouched MPS, the shading must be due to the contact between the indenter tip and MPS. We infer that the shaded area is the region of metal flattened by the indenter, and thus representative of the maximum extent of plastic deformation in the contact region.

The size of this area was determined using ImageJ, as illustrated in Figure 2. First the scale was set based on the scale bar from the SEM. The shaded area was then selected using the ellipsoid drawing tool. The area was calculated, and the contact radius by calculating the radius of an equivalent perfect circle with that area. In addition to the error source from the Hitachi S 5500 SEM calibration for size measurement, the method of drawing a circle by hand introduced uncertainties. By drawing the circle three times per contact area measurement and observing the variation of the measured area, we estimated this uncertainty to be ±1 $\mu m^2$. Further uncertainties stem from surface roughness and topographical gradient, which make it difficult to determine exactly where the contact area ends.

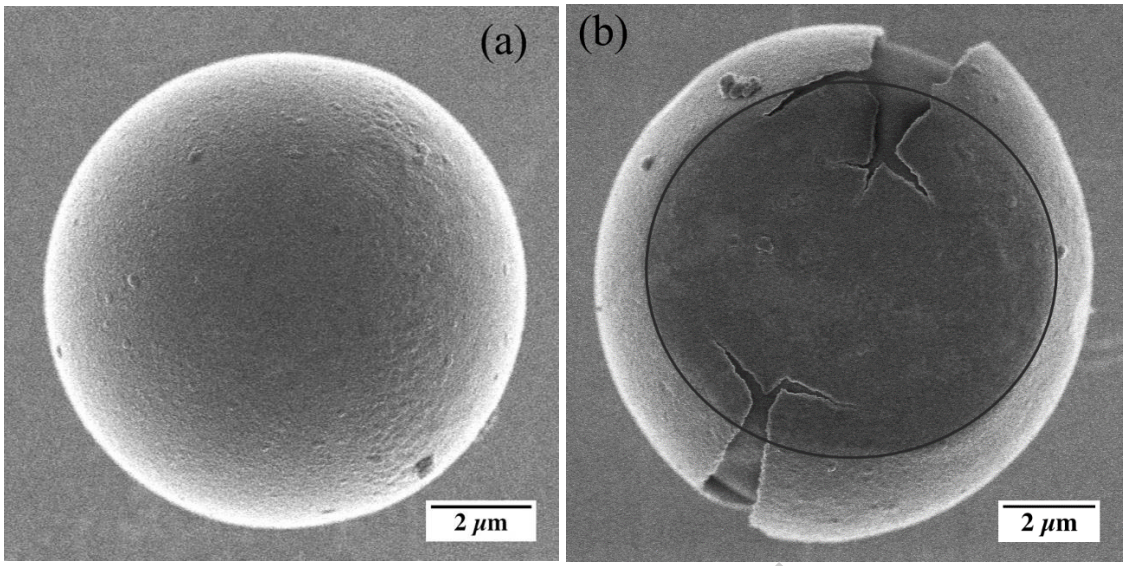


*Figure 2: Micrographs of (a) an untouched Ni90 and (b) a compressed Ni90 particle with the contact area encircled.*

### 3.4. Finite element model

To validate the experimental results, a FE model was created using COMSOL Multiphysics®, as shown in Figure 3. The purpose of the model was to investigate the influence of the thin metal coatings at the large strain studied experimentally.

An axisymmetric quarter-sphere was used to model the spherical geometry of the MPS. The MPS were modelled using a PMMA core in diameter of 10 μm and metal coating with a thickness corresponding to the particles measured, i.e. 40 – 120 nm. The coating is assumed to be homogenous, although it is in reality nanoscopically rough. The quarter-sphere was placed under a silicon plate, and the plate was incrementally stepped towards each other to simulate compression. This was to mimic the experimental set-up which was run in displacement control mode. Steps of 1 nm were performed up to 10 nm deformation, steps of 10 nm up to 100 nm deformation, steps of 100 nm up to 1000 nm deformation and 1000 nm up to 5000 nm deformation. We assume frictionless contact between the MPS and silicon plates; both literature and FE analyses have indicated that the coefficient of friction plays a negligible role in the resulting contact area [19,22].

The intrinsic material properties used are summarized in Table 1 below. To facilitate the simulation of large strains, a neo-Hookean hyperelastic model was applied to the polymer core while the metal coating was treated as an elastic-perfectly plastic material with linear isotropic hardening to improve convergence. The tangent modulus was set to be 0.02% of the initial Young's modulus. It should be noted that in both the elastic and elastic-plastic contact conditions, the contact area (Equations (1-3)) is independent of the elastic properties of the materials used. Details of the finite element analyses can be referred to our previous work [22]. Triangular elements were used, while the number of elements depended on the coating thickness since the meshing was finest in this area. A coarser mesh was used in the bulk of the polymer core. To verify the model, it was run as a linear

elastic only with the same material properties in the core and the coating. This yielded Hertzian contact behavior [1], as expected.

*Table 1: The material properties used in the FE model to obtain the contact area.*

| **Material** | **Young's Modulus [GPa]** | **Poisson Ratio** | **Yield strength [MPa]** |
|---|---|---|---|
| PMMA | 3 | 0.30 | N/A |
| Ni | 219 | 0.31 | 480 |
| Au | 70 | 0.44 | 170 |
| Ag | 83 | 0.37 | 66 |

The yield strength of nanoscale coatings may be different from the bulk values [33]. However, only bulk values of yield strength are readily available. A parametric analysis of the yield strength of gold was performed. The yield strength was systematically varied from 170 to 220 MPa. The average deviation of the contact radius – deformation curves from each other was < 0.3%. The absolute value of yield strength selected is therefore not found to be critical, and parameter corresponding to the bulk materials were selected.

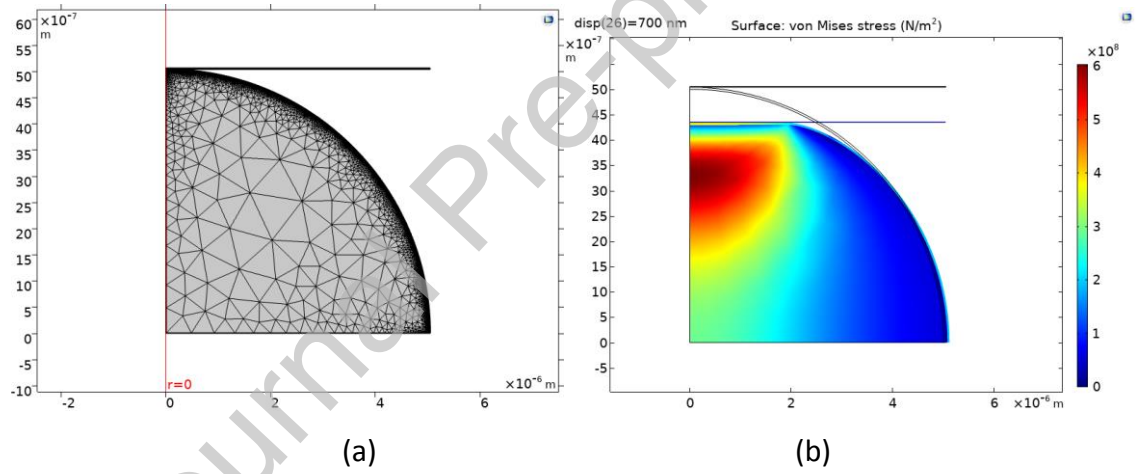


*Figure 3: (a) Schematics of the meshed quarter-sphere model, and (b) the resultant stress in the FEM used to validate the experimental results.*



## 4. Results and discussion

### 4.1. Force-deformation measurements

The nominal stress $\sigma$ and nominal strain $\varepsilon$ for an MPS are given by:

$$\sigma = \frac{F}{\pi {r_p}^2} \tag{4}$$

$$\varepsilon = \frac{\delta}{2r_p} \tag{5}$$

where $F$ is the applied force. Figure 4 shows representative stress-strain curves for each of the types of MPS examined, including both loading and unloading of the MPS. The Ni-coated MPS exhibit stress-drops during loading, which have been linked to brittle fracture events, while the Au and Ag MPS have monotonic loading curves. The loop around the stress drops indicates cracking, but the

magnitude of the stress drop is an artefact of the transducer attempting to maintain constant deformation rate with force actuation and not the result of material properties [34]. A thicker metal layer is generally expected to result in stiffer stress-strain response; we see in this case the opposite is true and the Ni90 is apparently stiffer than Ni120. This is not a systematic result, rather the particle-to-particle variation of the stiffness was observed to be large. The variations within one type of MPS are thus greater than any systematic effect of the metal thickness.

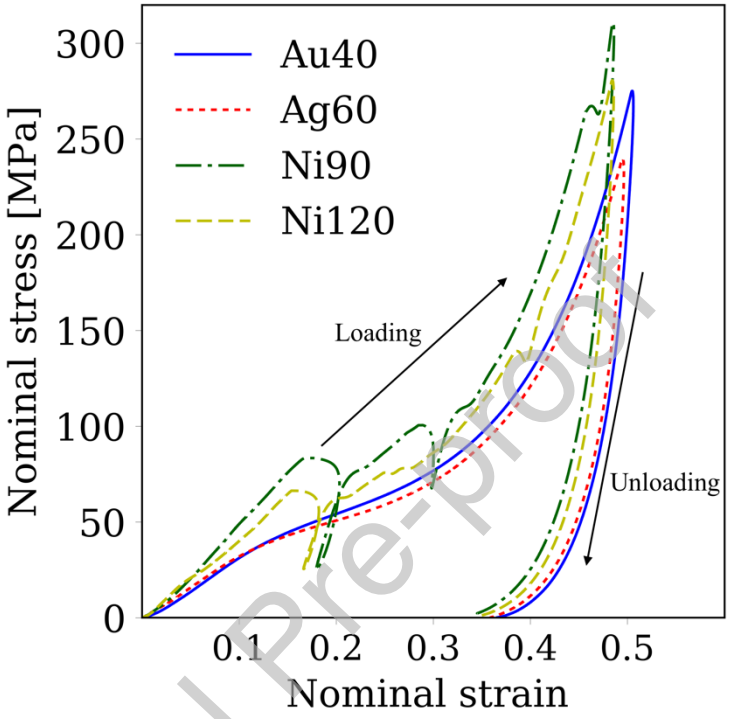


*Figure 4: A comparison of representative stress-strain characteristics of each type of MPS.*

The maximum strain was dictated by the maximum specified displacement, which was 5 µm for all the measurements in Figure 4. The maximum strain was always slightly below 0.5, since the measurement starts just above the particle. The unloading phase was similar for all particles. They recovered from nearly 0.5 strain to above 0.35 strain due to elastic recovery of the core. Since the cores are made of viscoelastic polymer, the cores are expected to recover further over time.

### 4.2. Contact area measurements

As the MPS are compressed, the contact area increases in a roughly circular manner from the first point of contact. Figure 5 shows representative SEM images of each MPS type, ordered by increasing maximum strain. The yield strength of metals is relatively low, so as the coating deforms plastically a fingerprint of the deformation is left behind. Although the polymer core recovers elastically (see Figure 4), we assume that recovery in the polymer core does not significantly influence the mark left from the indenter in the metal coating. The fingerprint is interpreted as a mark of the maximum achieved contact area. However, since some of the contact area will deform plastically, the contact area measured with this method is likely smaller than the true maximum contact area.

The contact area measurements were performed from images of the type shown in Fig. 5, based on the clear fingerprints left by the flat punch. A major trend is that Ni MPS (Figure 5 b & d) fracture in a brittle manner, with pronounced global delamination, while the Ag and Au MPS (Figure 5 a & c) deform in a ductile manner. This has been discussed in detail [34]. Previous simulation work has predicted that the fracture of the metal coating in MPS will initiate at the equator of the particle and propagate towards the contact area [36]. We were unable to confirm this directly since initiation and propagation progressed more quickly than the frame rate of imaging in the experiment. However, by comparing Figure 5 b & d, we can see that cracks stemming from higher strain extend further into the contact area, indicating that they are propagating towards and into, and not away from, the contact area. The open cracking regions in the Ni MPS do not decrease the available cross-section for electrical current conduction in application.

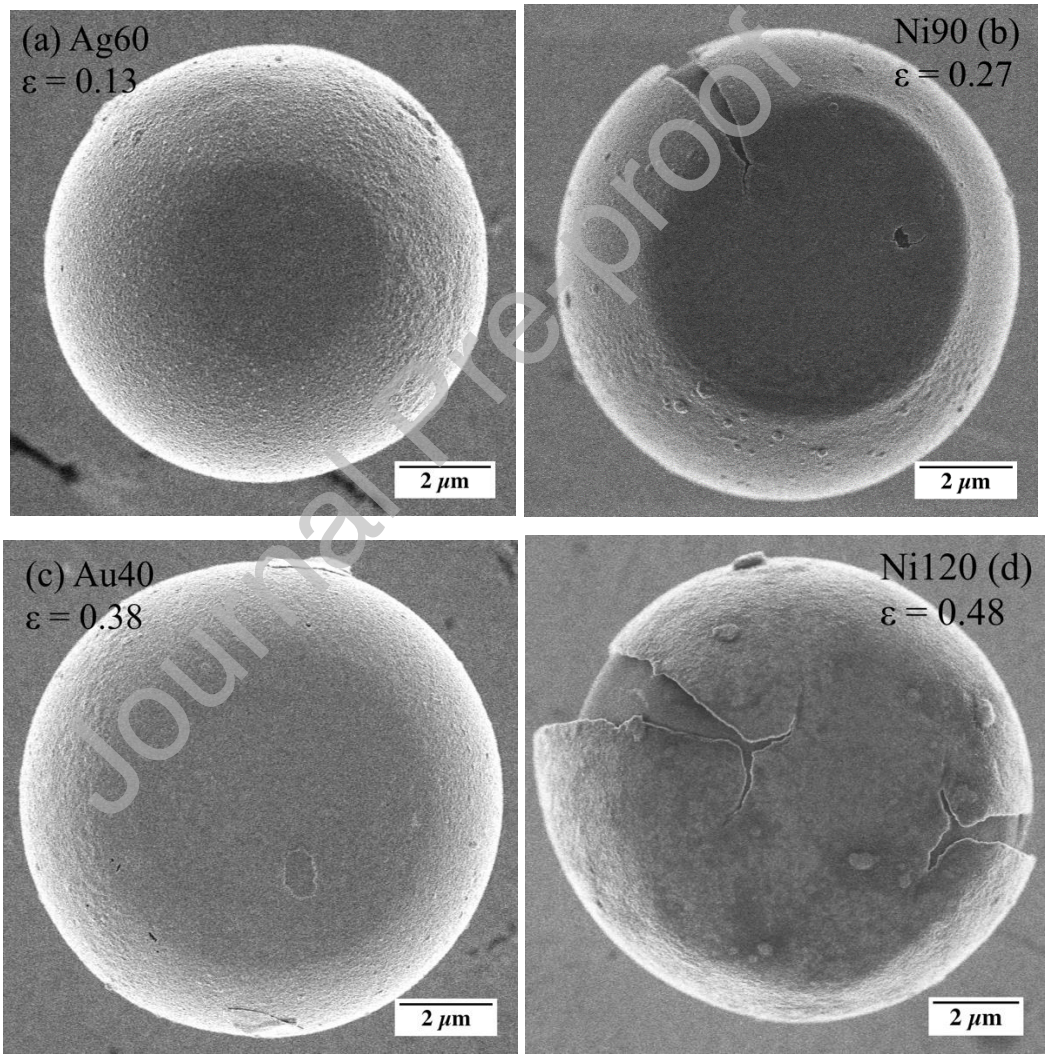


*Figure 5: SEM images of MPS deformed to varying degrees: (a) Ag60 after deformation to 0.13 strain; (b) Ni90 to 0.27 strain; (c) Au40 after deformation to 0.38 strain; (d) Ni120 to 0.48 strain.*

### 4.3. Comparison to contact area models

In Figure 6, the measured contact radius is plotted as a function of the Tatara radius (Eq. 1) for each type of MPS. The used of the Tatara radius in effect normalizes the deformation relative to the undeformed particle radius. The Tatara (elastic) and Abbott-Firestone (plastic) models as well as the FE results have been included for comparison. The radius of the polymer core, 4.85 µm, has been used as input for all models.

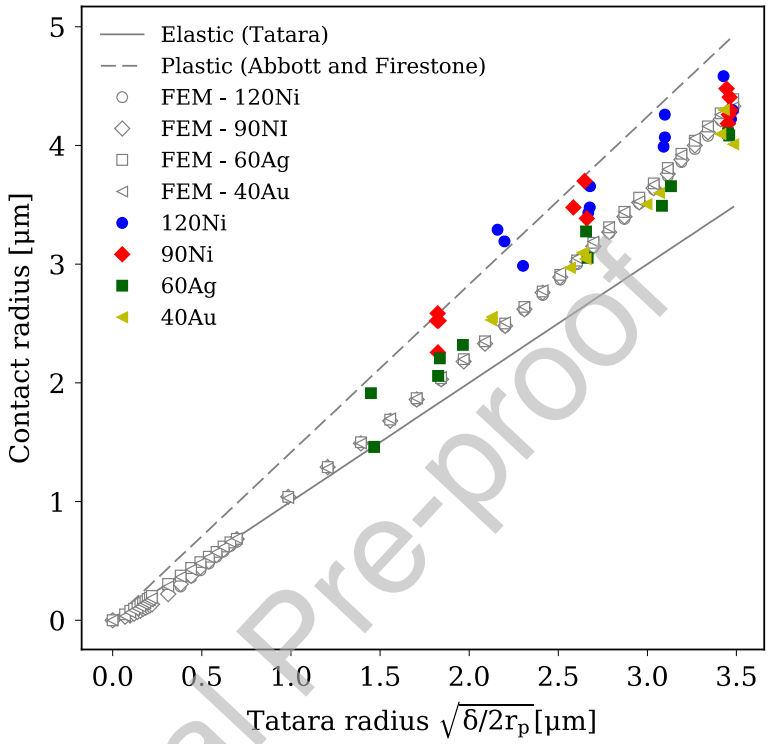


*Figure 6: The measured contact radius as a function of the Tatara contact radius.*

Although the measured contact radii for all particles follow a similar trend, the Ni MPS tend to have higher contact radius for a given Tatara radius. Both the FE results and the Tatara and Abbott-Firestone models predict a contact radius that is independent of material properties, so these models do not account for the observed discrepancy. As demonstrated in Figure 5, the Ni-coated MPS exhibit brittle fracture, a phenomenon not accounted for in the FE model. During brittle fracture, the indentation transducer is unable to maintain constant deformation rate, resulting in the loops visible in Figure 4. The abrupt increase in deformation causes a corresponding increase in contact area, which could explain the larger contact area in Ni system in Figure 6.

As can be seen in Figure 6, experimental data falls between the elastic and plastic models. Since the measured contact area is residual, it must be the result of some degree of plastic deformation. However, the polymer core has a high cross-linking density and will thus tend of deform elastically [21]. Since both types of deformation occur, it is logical that the contact area falls somewhere between the elastic and plastic estimates.

The contact area predicted by the FE model does not vary significantly with the coating thickness or mechanical properties of the metal within the range tested in this study, although it is in good agreement with the experimental data. This is likely because the range of thicknesses examined is relatively small. The FE model tends to underestimate the contact area, so plastic deformation of the core could be implemented to obtain a more accurate contact area predicted, as will be the topic of a future study.

With the current experimental setup, we were unable to observe the contact area on MPS deformed to less than 500 nm. This indicates a threshold below which no plastic deformation of the metal occurs, and it is possible that the contact area during compression was slightly larger than the measured contact area if there is a region of elastic deformation around the perimeter. Previous work found mostly elastic deformation up to the point the coating fracture point of Ni/Au MPS [35].

We further consider the force-contact area relationship. According to Eq. 3, the applied force should be directly proportional to the real contact area and the slope should represent $\xi H$, where $H$ is the contact hardness. Although we have measured the apparent rather than real contact area, it is interesting to see if a linear relation exists. The measured contact area versus applied force is plotted in Figure 7. The data is *not* linear throughout the measurement range. The relation between the real and apparent contact area must thus be non-linear if Holm's theory is to hold for the real contact area. We postulate that the apparent contact area is dictated by the polymer core, while the real contact area is dictated by the (local) hardness of the metal coating.

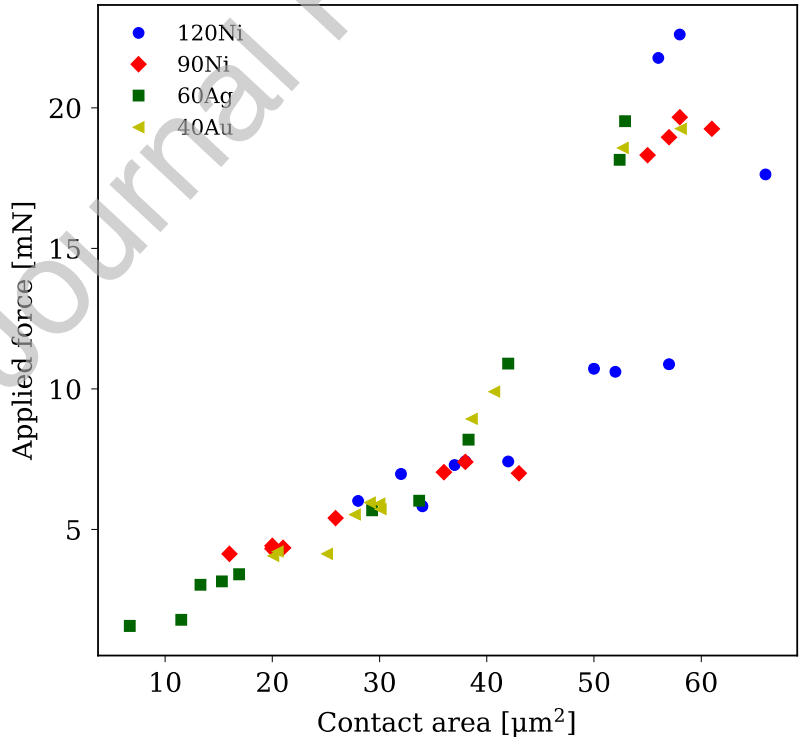


*Figure 7: The maximum applied force as a function of the measured contact area.*

The main result is that the apparent, measured contact area principally depends on the absolute deformation for the relatively thin metal systems studied in the work, and that the Tatara theory is a good indicator of the expected contact area in MPS. In terms of ACA applications, a large contact area is generally advantageous in terms of minimizing contact resistance. ACA bonding applications function in terms of applied force, and as we can see in Figure 7 the data does not show a significant difference in the contact area as a function of force for the different metal systems. However, the real (current carrying) contact area may be significantly different from the apparent contact area, and cannot be estimated by the techniques used in this work.

## 5. Conclusion

The force, deformation and resultant contact area of 10 µm Ni, Au and Ag coated polymer particles were measured using a flat punch nanoindentation technique with in-situ SEM observation. The goal was to understand the evolution of the contact area at large deformations, which is relevant for anisotropic conductive adhesive (ACA) applications and otherwise undocumented in the literature. We find that the metal coating metallization and thickness do not significantly influence the development of the contact area, although all the studied coatings are relatively thin. The contact area evolution only depends on the absolute deformation and particle size, and is independent of material properties. The contact area falls between elastic and plastic models, indicating that both types of deformation occur. Although the contact area evolution is similar in all the systems studied, we note that this is the apparent contact area and may not reflect the true, current carrying area that determines the contact resistance.



## Acknowledgements

The authors would like to thank Haiyan Song for fabrication of MPS samples, and Bertil Nistad and the COMSOL support team for input to the FE model. The Research Council of Norway is acknowledged for funding through projects New manufacturing technology for ACF (grant No. 245432). Partial funding has also been obtained from the Programme FP7-NMP-2013-LARGE-7 under grant agreement n604668 (QuantiHeat).

## References

[1] Hertz H. Ueber die Berührung fester elastischer Körper. J Für Die Reine Und Angew Math 1882;92:156–71.

[2] Paul J, Romeis S, Tomas J, Peukert W. A review of models for single particle compression and their application to silica microspheres. Adv Powder Technol 2014;25:136–53. doi:10.1016/j.apt.2013.09.009.

[3] Goltsberg R, Etsion I. Contact area and maximum equivalent stress in elastic spherical contact with thin hard coating. Tribol Int 2015;93:289–96. doi:10.1016/j.triboint.2015.09.034.

[4] Kogut L, Etsion I. Elastic-Plastic Contact Analysis of a Sphere and a Rigid Flat. J Appl Mech 2002;69:657. doi:10.1115/1.1490373.

[5] Lin YC, Zhong J. A review of the influencing factors on anisotropic conductive adhesives joining technology in electrical applications. J Mater Sci 2008;43:3072–93. doi:10.1007/s10853-007-2320-4.

[6] Yim MJ, Paik KW. The contact resistance and reliability of anisotropically conductive film (ACF). IEEE Trans Adv Packag 1999;22:166–73. doi:10.1109/6040.763188.

[7] Chin M, Barber JR, Hu SJ. Effect of elastic recovery on the electrical contact resistance in anisotropic conductive adhesive assemblies. IEEE Trans Components Packag Technol 2006;29:137–44.

[8] Chan YC, Luk DY. Effects of bonding parameters on the reliability performance of anisotropic conductive adhesive interconnects for flip-chip-on-flex packages assembly II. Different bonding pressure. Microelectron Reliab 2002;42:1195–204. doi:10.1016/S0026-2714(02)00089-6.

[9] Ghaednia H, Wang X, Saha S, Xu Y, Sharma A, Jackson RL. A Review of Elastic-Plastic Contact Mechanics. Appl Mech Rev 2017. doi:10.1115/1.4038187.

[10] He JY, Zhang ZL, Midttun M, Fonnum G, Modahl GI, Kristiansen H, et al. Size effect on mechanical properties of micron-sized PS–DVB polymer particles. Polymer (Guildf) 2008;49:3993–9. doi:10.1016/j.polymer.2008.07.015.

[11] He JY, Nagao S, Kristiansen H, Zhang ZL. Loading rate effects on the fracture of Ni/Au nano-coated acrylic particles. Express Polym Lett 2012;6:198–203. doi:10.3144/expresspolymlett.2012.22.

[12] He JY, Zhang ZL, Kristiansen H. Compression properties of individual micron-sized acrylic particles. Mater Lett 2013;63:1696–8. doi:10.1016/j.matlet.2009.05.013.

[13] Bazilchuk MS, Pettersen SR, Kristiansen H, Zhang ZL, He JY. Electromechanical characterization of individual micron-sized metal coated polymer particles. J Appl Phys 2016;119. doi:10.1063/1.4954218.

[14] Bettscheider S, Gachot C, Rosenkranz A. How to measure the real contact area? A simple marker and relocation foot-printing approach. Tribol Int 2016;103:167–75. doi:10.1016/j.triboint.2016.06.034.

[15] Ovcharenko A, Halperin G, Etsion I, Varenberg M. A novel test rig for in situ and real time optical measurement of the contact area evolution during pre-sliding of a spherical contact. Tribol Lett 2006;23:55–63. doi:10.1007/s11249-006-9113-9.

[16] Bazilchuk M, Evenstad OM, Zhang Z, Kristiansen H, Jianying He. Resistance analysis of spherical metal thin films combining van der pauw and electromechanical nanoindentation methods. Submitt to J Electron Mater n.d.

[17] Xu Y, Chen Y, Zhang A, Jackson RL, Prorok BC. A New Method for the Measurement of Real

Area of Contact by the Adhesive Transfer of Thin Au film. Tribol Lett 2018;66:1–20. doi:10.1007/s11249-018-0982-5.

[18] Chang WR, Etsion I, Bogy DB. An Elastic-Plastic Model for the Contact of Rough Surfaces. J Tribol 1987;109:257. doi:10.1115/1.3261348.

[19] Chen Z, Goltsberg R, Etsion I. A universal model for a frictionless elastic-plastic coated spherical normal contact with moderate to large coating thicknesses. Tribol Int 2017;114:485–93. doi:10.1016/j.triboint.2017.05.020.

[20] Chen Z, Goltsberg R, Etsion I. Plasticity evolution in a coated sphere compressed by a rigid flat. Tribol Int 2016;98:116–24. doi:10.1016/j.triboint.2016.02.004.

[21] He JY, Zhang ZL, Kristiansen H, Redford K, Fonnum G, Modahl GI. Crosslinking effect on the deformation and fracture of monodisperse polystyrene-co-divinylbenzene particles. Express Polym Lett 2013;7:365–74. doi:10.3144/expresspolymlett.2013.33.

[22] Zhang ZL, Kristiansen H, Liu J. A method for determining elastic properties of micron-sized polymer particles by using flat punch test. Comput Mater Sci 2007;39:305–14. doi:10.1016/j.commatsci.2006.06.009.

[23] Tatara Y. On compression of rubber elastic sphere over a large range of displacements—part 1: theoretical study. J Eng Mater Technol 1991;113:285–91.

[24] Johnson KL. Adhesion at the contact of solids. Theor Appl Mech 1977:133–43.

[25] Abbott EJ, Firestone FA. Specifying surface quality. Mech Eng 1933;55:569–72.

[26] Yu H, Kongsmo R, Patil N, He JY, Breiby DW, Zhang ZL. On determining the Poisson's ratio of viscoelastic polymer microparticles using a flat punch test. Int J Mech Sci 2017;128–129:150–8. doi:10.1016/j.ijmecsci.2017.04.019.

[27] Hunter SC. The Hertz problem for a rigid spherical indenter and a viscoelastic half-space. J Mech Phys Solids 1960;8:219–34. doi:10.1016/0022-5096(60)90028-4.

[28] Lee EH, Radok JRM. The Contact Problem for Viscoelastic Bodies 2018:438–44.

[29] Graham GAC. The contact problem in the linear theory of viscoelasticity when the time dependent contact area has any number of maxima and minima. Int J Eng Sci 1967;5:495–514. doi:10.1016/0020-7225(67)90037-7.

[30] Timsit RS. Electrical contact resistance: Properties of stationary interfaces. IEEE Trans Components Packag Manuf Technol Part A 1999;22:194–9.

[31] Constable JH. Analysis of ACF contact resistance. IPACK03, 2003, p. 1–8.

[32] Holm R. Electric Contacts: Theory and application. 4th ed. Springer; 1967.

[33] Espinosa HD, Prorok BC, Peng B. Plasticity size effects in free-standing submicron polycrystalline FCC films subjected to pure tension. J Mech Phys Solids 2004;52:667–89. doi:10.1016/j.jmps.2003.07.001.

[34] Bazilchuk MS, Sumigawa T, Kitamura T, Zhang ZL, Kristiansen H, He JY. Deformation and fracture of micron-sized metal-coated polymer spheres: an in situ study. Adv Eng Mater 2018.

doi:201800049.

[35] He JY, Helland T, Zhang ZL, Kristiansen H. Fracture of micrometre-sized Ni/Au coated polymer particles. J Phys D Appl Phys 2009;42:085405. doi:10.1088/0022-3727/42/8/085405.

[36] Xie B, Shi XQ, Ding H, Member S. Investigation of Mechanical and Electrical Characteristics for Cracked Conductive Particle in Anisotropic Conductive Adhesive ( ACA ) Assembly. IEEE Trans Components Packag Technol 2008;31:361–9.